Available online at www.sciencedirect.com
ScienceDirect
Trans. Nonferrous Met. Soc. China 26(2016) 1345−1352
Transactions of Nonferrous Metals Society of China
www.tnmsc.cn

Effect of TiO_2 and ZrO_2 reinforcements on properties of Al_2O_3 coatings fabricated by thermal flame spraying

Rassim YOUNES[1], Mohand Amokrane BRADAI[1], Abdelhamid SADEDDINE[1],
Youcef MOUADJI[2], Ali BILEK[3], Abderrahim BENABBAS[4]

1. Laboratory of Mechanics, Materials and Energetic, Faculty of Technology, University of Bejaia, 06000 Bejaia, Algeria;
2. Laboratory of Mechanics, Faculty of Engineering Sciences, Campus Chaabet-Ersas, University of Constantine, 25000 Constantine, Algeria;
3. Mechanical Laboratory of Structure and Energetic, Mechanical Engineering Department, University of Tizi-Ouzou, 15000 Tizi-Ouzou, Algeria;
4. Laboratory Processes for Materials, Energy, Water and Environment, Faculty of Science and Technology, University of Bouira, 10000 Bouira, Algeria

Received 30 April 2015; accepted 11 September 2015

Abstract: The alumina composite coatings reinforced with 25% ZrO_2 (denoted as AZ-25) and 3% TiO_2 (denoted as AT-3) were deposited on low carbon steel using a thermal flame spraying. The microstructure, phase composition, microhardness and tribological properties of the coatings were investigated. The XRD results of the coatings reinforced by TiO_2 (AT-3) revealed the presence of α-Al_2O_3 phase as matrix and new metastable phases of γ-Al_2O_3 and κ-Al_2O_3. However, the coatings reinforced by ZrO_2 (AZ-25) consist of α-Al_2O_3 as matrix, q-ZrO_2 and m-ZrO_2. In most studied conditions, the AT-3 coating displays a better tribological performance, i.e., lower coefficient of frictions and wear rates, than the AZ-25 coating. It was also found that the microhardness of the coatings was decreased with the reinforcement of ZrO_2 and increased with TiO_2.
Key words: thermal spraying; coatings; reinforcements; friction coefficient; wear rate

1 Introduction

Thermal spray allows to produce coatings up to several millimeters thickness. It can also be used to recover worn machinery parts that can be mechanized afterwards. This technique also makes it possible to deposit ceramics, polymers and metals as well as composite materials on many different substrates [1,2]. Thermal spray coatings, which consist of a lamellar structure of flattened and solidified fine particles, are porous [3]. It involves introducing solid particles (wire or powder) in a flame or plasma jet to melt and accelerate them before they come crashing on the substrate where they form a multilayer [4−6]. Hard ceramic coatings are important candidates for anti-wear and anti-corrosion applications which are exposed to very harsh environments [7−11]. Many researchers focused on enhancing the mechanical properties of coatings by the addition of a ceramic phase as TiO_2 [12−20] and ZrO_2 [21−24]. Understanding the relationships between different physical properties and microstructure was the main cause of research to improve the mechanical properties of these composites. Improving the tensile strength and toughness of alumina matrix nanocomposites was observed and explained by the combination of Hall-Petch effect due to nanoparticles [25−29]. In contrast, studies on tribological ceramic matrix composites containing ceramic or metallic nanoparticles are few. However, alumina is the most widely used material as a matrix [30−32].

Alumina ceramic has very high hardness and good strength but relatively low toughness in comparison with zirconia, which exhibits very high strength and good toughness but shows relatively poor hardness. The strength and toughness of alumina may be enhanced by

Corresponding author: Mohand Amokrane BRADAI; Tel/Fax: +213-34-21-51-05; E-mail: mokbrad@yahoo.fr
DOI: 10.1016/S1003-6326(16)64237-1

dispersion of zirconia solid solutions, mainly due to the tetragonal monoclinic transformation [33−36]. Strength and toughness of zirconia dispersed ceramics are strongly affected by: 1) the amount of tetragonal zirconia phase (t-ZrO_2) retained in the body, and 2) the compositional variation and critical size of dispersed zirconia [37,38].

FERVEL et al [39] reported that the coatings wear resistance achieved by plasma deposition from the Al_2O_3−40%TiO_2 powder (AT-40) was higher than that of deposits developed using powders of Al_2O_3−13%TiO_2 (AT-13). In contrary, HABBIB et al [40] concluded that the higher hardness of coatings (AT-13) obtained by oxyacetylene flame was because these coatings were more resistant to abrasive wear by sliding contact such as those developed with powders AT-40. In another study, AHN et al [41] found that low wear resistance of coatings (AT-13) made with conventional micrometric powders is due to the presence of brittle phases from titanium oxide produced between the splats of multilayers.

The present investigation was conducted to study the tribological properties of Al_2O_3 matrix coatings reinforced with 3% TiO_2 and 25% ZrO_2 (mass fraction), namely (AT-3) and (AZ-25) respectively. The tribological tests were carried out using a pin-on-disc tribometer at different loads. All tests were performed using a disc as counter body namely Al_2O_3−13%TiO_2 (AT-13), which formed couple 1 and couple 2 respectively, in order to work out the wear rate and friction coefficient. The microstructural and structural characterization of the as-received feedstock wires and coatings was obtained by scanning electron microscopy (SEM) and X-ray diffraction (XRD). The choice of these ceramic coatings is to improve the wear resistance of the renovated mechanical parts to give them a new technical life despite its previous degradation in service. The phase structure, elements distribution and microhardness of the coatings are studied. The influence of the applied load and sliding time on the friction coefficient and wear resistance of the coatings is discussed as two contact couples:

Couple 1: Pin coated with Al_2O_3−25%ZrO_2 (AZ-25)/ceramic disc Al_2O_3−13%TiO_2 (AT-13);

Couple 2: Pin coated with Al_2O_3−3%TiO_2 (AT-3)/ ceramic disc Al_2O_3−13%TiO_2 (AT-13).

2 Experimental

2.1 Materials and spraying process

The substrate used in the present work was an E335 steel. The chemical composition (mass fraction, %) obtained by using X-ray fluorescence is balanced Fe, 0.2% Cu, 0.1%−0.15% C, <0.05% Ni, 0.2%−0.25% Mn. It was machined to the cylindrical geometry with 10 mm in diameter and 20 mm in length. Before the coating process, blasting was conducted at a pressure of 0.4 MPa and a distance of 150 mm for 60 s with alumina grit of 99.50% purity and 0.5 mm mean particle size. The surface was then cleaned and degreased using acetone in an ultrasonic bath. The chemical composition of coatings and disc used as counter body in tribological tests are shown in Table 1.

Table 1 Chemical composition of materials used (mass fraction, %)

Material	Al_2O_3	TiO_2	ZrO_2	Others
Disc (AT-13)	87	12.7	−	0.3
Coating (AZ-25)	75	−	24.5	0.5
Coating (AT-3)	97	2.8	−	0.2

Oxy-acetylene thermal spray gun flame-wire from Master-Jet Gun 2 was used with low speed electric motors (10 mm/s) for driving the wire. This combination provides a thermal power of 24 kW by mixing oxygen at 4 MPa with acetylene at 1.2 MPa. The main parameters used were: spraying distance of 120 mm, spray angle of 90° and a gun displacement over the sample surface of 25 mm/s. The pressure of air was 4.5 MPa. The average speed particle was 300 m/s. The spray gun was passed over each sample to obtain coatings up to 1 mm thickness. Substrates were heated at 200 °C before thermal spraying to increase the adherence of the coating to the substrates.

2.2 Surface analysis

The surface of samples was ground using SiC paper with grit sizes and finally polished with alumina. Microstructures of the initial wires and produced coatings were observed on its surface using a scanning electron microscope (SEM) from Japanese (JEOL JSM−6360LV) in high vacuum.

The X-ray diffraction patterns were recorded at room temperature with a X’Pert PRO MRD Diffractometer of PANalytical equipped with a Cu-anode X-ray tube and a curved graphite monochromator in the diffracted beam set of Cu K_α radiation which includes the $K_{\alpha 1}$ and $K_{\alpha 2}$ wavelengths. The strong presence of defects in these materials creates a significant background noise; to improve counting statistics and increase the peak/background ratio, an acquisition time of 40 s was used per angular step of 0.04° over the 20°−90° (2θ) range. The identification of the crystal phases present in the coatings was performed using X’Pert HighScore software supported with the ICDD-PDF2 database.

2.3 Microhardness test

The mechanical properties of the materials were investigated by a kind of continuous Vickers hardness test. The surface of the coatings and samples was mechanically polished before measurement. During the test a Vickers pyramid was pressed into the surface of the sample by controlled hydraulic mechanical testing machine Zeiss. During the loading period, the Vickers pyramid penetrated into the surface of the sample at constant velocity and the same velocity was applied in the unloading period when the pyramid moved backwards. The indentation procedure consisted of 60 steps, with a waiting period between consecutive steps of 30 s according to ASTM 1327 [42]. Hardness measurements were performed under indentation loading of 2 N. An average hardness was calculated from 10 indents per specimen. Measurements were performed on various materials: metal substrate E335, counter body disc (AT-13) and two alumina coatings reinforced by ZrO_2 (25%) and TiO_2 (3%).

2.4 Tribological behavior

Tribological tests were carried out in a pin-on-disc tribometer at room temperature of 25 °C. The coatings slid against the discs under dry friction at the loads of 5, 10, 15, 20 and 30 N with a sliding distance of 1000 m in the duration of 30 min, sliding speed of 0.5 m/s and a wear track diameter of 3 cm. The coated steel substrate, formed the pins in the system, was machined into cylinders of 10 mm in diameter and 20 mm in length. A ceramic disc of 30 cm in diameter was employed as the counter body with a new disc being used for each test. Both pin and disc samples were cleaned with ethanol and dried by compressed air before and after testing. In order to study the wear behaviour of coatings in severe conditions, the tests were carried out without any lubrification. The wears experienced by the samples during the tests were determined by weighing each sample before and after the test. Friction coefficients were tested by the software attached to tribometer pin on disc. Wear losses were measured using a TG328B balance having an accuracy of ±0.01 mg. The wear rate is calculated using the following equation:

$$K_{\mathrm{v}}=\frac{\Delta m}{N_{\mathrm{c}}} \quad (1)$$

where K_{v} is the wear rate; Δm is the mass loss; N_{C} is the number of cycles.

The value of the static friction coefficient is obtained by the equation below:

$$\mu=\frac{F_t}{N} \quad (2)$$

where F_{t} is the tangential force; N is the normal force.

Tribological tests were performed according to two contact couples:

Couple 1: Pin coated with Al_2O_3−ZrO_2 (AZ-25)/disc Al_2O_3-TiO_2 (AT-13);

Couple 2: Pin coated with Al_2O_3−TiO_2 (AT-3)/disc Al_2O_3-TiO_2 (AT-13).

3 Results and discussion

3.1 Microstructure characterization

3.1.1 Microstructure of as-received feedstock wires

Figure 1 shows the morphologies of the two as-received feedstock wires. It can be seen that the Al_2O_3−3%TiO_2 (AT-3) particles show an irregular and angular morphology, which is confirmed by the internal morphology of Al_2O_3 composite wire as shown in Fig. 1(a). Also, the SEM morphology of Al_2O_3−25%ZrO_2 (AZ-25) particle (Fig. 1(b)) shows that the agglomerated wire had granular shape and was more compact than AT-3. It was demonstrated that the ultra-fine grains were closely connected with each other, which could be due to the sintering effect and would contribute to improve the strength.

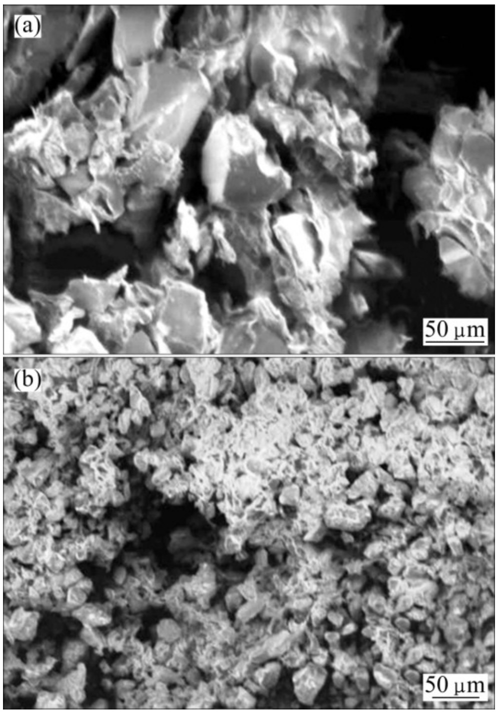

Fig. 1 SEM images of wire: (a) Al_2O_3−3%TiO_2 (AT-3); (b) Al_2O_3−25%ZrO_2 (AZ-25)

3.1.2 Characterization of coatings

The SEM observations of the coating Al_2O_3−3%TiO_2 (AT-3) obtained by oxyacetylene flame spray showed a dense, compact and complex microstructure of several phases with the presence of porosities and unmelted particles (Fig. 2(a)). This microstructure is constituted by lamellae and globular pores and has no cracks because the stresses produced during the formation of these multilayers are not sufficient to produce it. Also, the coating has low porosity which can be associated with the effect of the higher speed in flight reaching the particles from the wire and due to the high pressure air jet and thus higher impact speed, resulting in better spreading lamellae. But the SEM image of the coating Al_2O_3−25%ZrO_2 (AZ-25) presents compact and complex microstructure of several phases with the presence of porosities, and this microstructure is constituted by lamellae splats that form à blocky structure. The zirconia inclusions are distributed uniformly within the composites. The ZrO_2 particles are mainly located at the grain boundaries of alumina, so the microstructure of alumina is refined due to the pinning effect exerted by the zirconia particles.

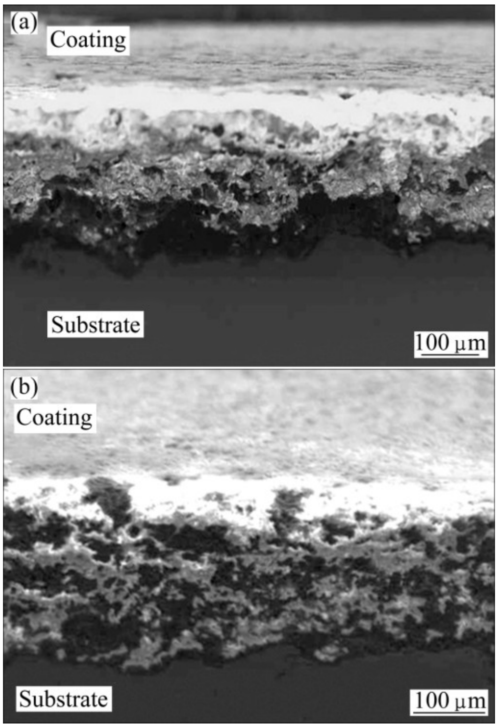

Fig. 2 SEM images of as-sprayed coatings: (a) Al_2O_3−3%TiO_2 (AT-3); (b) Al_2O_3−25%ZrO_2 (AZ-25)

3.2 XRD analysis

Figure 3 shows the XRD patterns of the wire alumina (Al_2O_3) matrix reinforced by titania (3% TiO_2) and the coating obtained by spraying flame-wire.

Figure 3(a) shows the diffractogram obtained from the wire Al_2O_3−TiO_2 (AT-3). The observed peaks reveal the presence of three phases: a majority phase of α-Al_2O_3 with rhombohedral structure (JCPDS No. 046-1212), the secondary phase of $Al_6Si_2O_{13}$ with orthorhombic structure (JCPDS No.015-0776) and small amount of rutile α-TiO_2 orthonombic structure (JCPDS No. 023-1446). The XRD pattern of Al_2O_3−TiO_2 (AT-3) coating (Fig. 3(b)) also reveals the presence of α-Al_2O_3 as matrix and new phases of γ-Al_2O_3 (JCPDS No. 01-074-2206) and κ-Al_2O_3 (JCPDS No. 046-1215), but the α-TiO_2 phase had disappeared. The crystalline parameter of this new cubic phase γ-Al_2O_3 is a=7.9060 Å. Indeed, the time of elaboration of the coating from the wire Al_2O_3−TiO_2 isn't enough to form oxides of titanium or others phases that contain Ti atoms. The Ti atoms are dissolved in phase γ-Al_2O_3 or κ-Al_2O_3 [43−45].

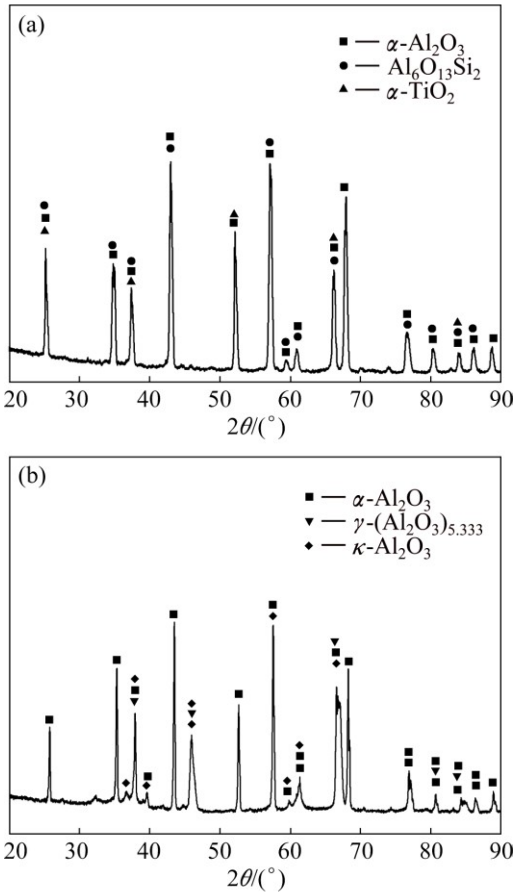

Fig. 3 XRD patterns of Al_2O_3−3%TiO_2 (AT-3): (a) Wire; (b) Coating

Figure 4 shows the diffraction patterns of the wire alumina (Al_2O_3) matrix reinforced by zirconia (25% ZrO_2) and the coating obtained by spraying flame-wire.

Apart from peaks corresponding to alumina−zirconia (Figs. 4(a) and (b)), it shows that the reaction of combustion in the flame gun transformed wire to α-Al_2O_3 and ZrO_2 completely. It can be concluded that a composite coating containing Al_2O_3 and ZrO_2 is formed by the same phases constituted the wire: α-Al_2O_3 matrix, monoclinic structure ZrO_2 (JCPDS No. 01-078-0047) and a quadratic structure ZrO_2 (JCPDS No. 01-088-1007). The reinforcement of alumina with zirconium improves the mechanical properties of the coating by the formation of the quadratic ZrO_2 [46,47]. The presence of amorphous phases is inevitable in the coating process; it is inherent to the more or less fast cooling of the sprayed particles. Nevertheless, their percentages in our alumina coatings remain limited in view of the background shape in the corresponding XRD diagrams; in addition, it will be noted in particular that the use of zircon favors this tendency through the partial substitution of Al^{3+} ions by the more charged and larger Zr^{4+} ions. The qualitative and quantitative analyses of these amorphous parts require further study through more refined XRD diagrams and SEM/EDS data.

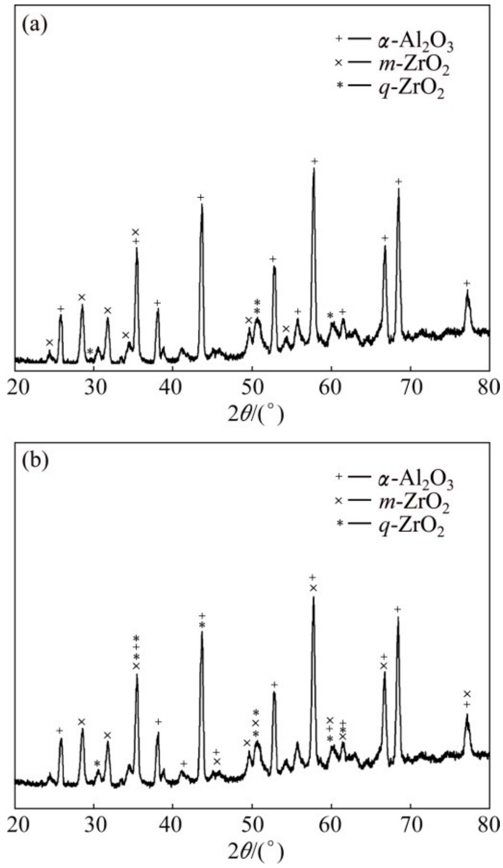

Fig. 4 XRD patterns of Al_2O_3−25%ZrO_2 (AZ-25): (a) Wire; (b) Coating

3.3 Vickers hardness

The micro hardnesses of the various materials used (substrate E335, disc which forms the contact couples Al_2O_3−TiO_2 (AT-13) and Al_2O_3−TiO_2 (AT-3) and Al_2O_3−ZrO_2 (AZ-25) coatings) were measured by Vickers indentation with a load of 200 g with duration time of 30 s. For each processing, the calculated average standard deviation is based on the average of 10 measurements. The results of Vickers pyramid hardness are illustrated in Fig. 5. Also, the curves of load−displacement of Vickers hardness test can be drawn using a model proposed by IANKOV et al [48]. Figure 6 illustrates the residual imprint image of as-sprayed coatings under load of 200 g during 30 s for the two coatings.

These tests revealed that the microhardness of the Al_2O_3−TiO_2 (AT-3) coating is three times larger than that of antagonist coating of Al_2O_3−ZrO_2 (AZ-25): $HV_{0.2}$ 1280±66 (AT-3) against about $HV_{0.2}$ 563±25 (AZ-25). This gap can be due to the influence of the quantity of porosity and difference between the hardness of reinforcement elements of titanium for Al_2O_3−TiO_2 and zirconium for Al_2O_3−ZrO_2. However, the microhardness value of Al_2O_3−TiO_2 (AT-3) coating is nearly equal to that of other antagonist disc of coating Al_2O_3−TiO_2 (AT-13): $HV_{0.2}$ 1280±66 (AT-13) against $HV_{0.2}$ 1326±64 (AT-3). In principle, the microhardness of Al_2O_3−TiO_2 coatings depends essentially on their composition; decreasing linearly with the TiO_2 content [46]. The phases in the Al_2O_3−TiO_2 (AT-13) coating are mainly composed of both alpha alumina (α-Al_2O_3) and gamma alumina (γ-Al_2O_3) while Al_2TiO_5 phase has lower hardness and mechanical resistance than alpha and gamma alumina [49−52].

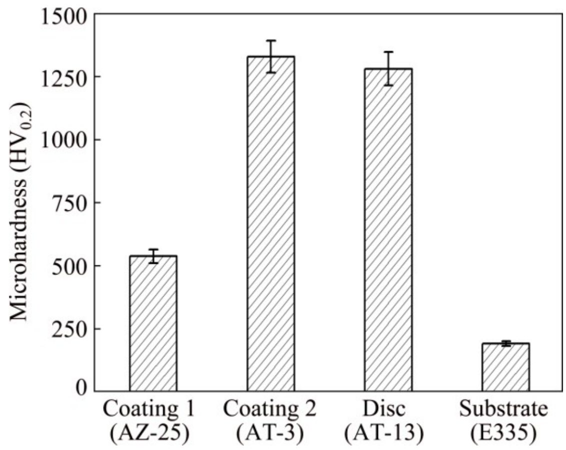

Fig. 5 Microhardness of different materials used

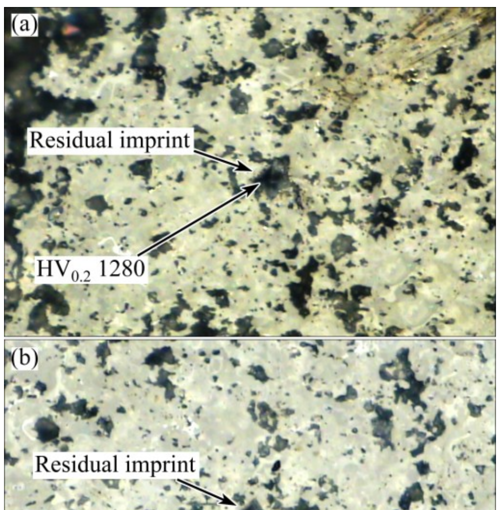

Fig. 6 Residual imprint images of as-sprayed coatings: (a) Al_2O_3−3%TiO_2 (AT-3); (b) Al_2O_3−25%ZrO_2 (AZ-25)

3.4 Tribological behaviour

Both Al_2O_3−TiO_2 (AT-3) and Al_2O_3−ZrO_2 (AZ-25) coatings against counter body Al_2O_3−TiO_2 (AT-13) tests were performed on pin-on-disc tribometer with sliding speed 0.5 m/s at different loads (5 N and 30 N) in order to determine the wear rate and the coefficient of friction. Figure 7 shows the variation of the friction coefficient of the two couples as function of sliding time at loads of 5 N and 30 N. The tribological results showed that the two curves are nearly identical during the first 5 min under applied loads of 5 N and 30 N. This transition phase can be explained by the presence of asperities which generate a tangential resistant force being next to the normal force. After this phase, the coatings reinforced by TiO_2 and ZrO_2 gave the same average friction coeffcient of about 0.92 under load 5 N. When they slid under 30 N, the friction coefficient obtained from the coatings reinforced by TiO_2 is higher than that of the coatings reinforced by ZrO_2 (0.65 for Al_2O_3−TiO_2 (AT-3) against 0.45 for Al_2O_3−ZrO_2 (AZ-25) (Figs. 7(a) and (b)). Through these results, we can conclude that the type of reinforcement in alumina coatings affects the tribological properties. Indeed, the reinforcement of TiO_2, which increases the microhardness of the matrix, increases the shearing force that causes a high friction coefficient. In contrary, the zirconia reinforcement decreases the microhardness of the alumina coatings and the friction coefficient, thus generates a sliding mode. From this, we can say that the pressure affects the variation of friction coefficient.

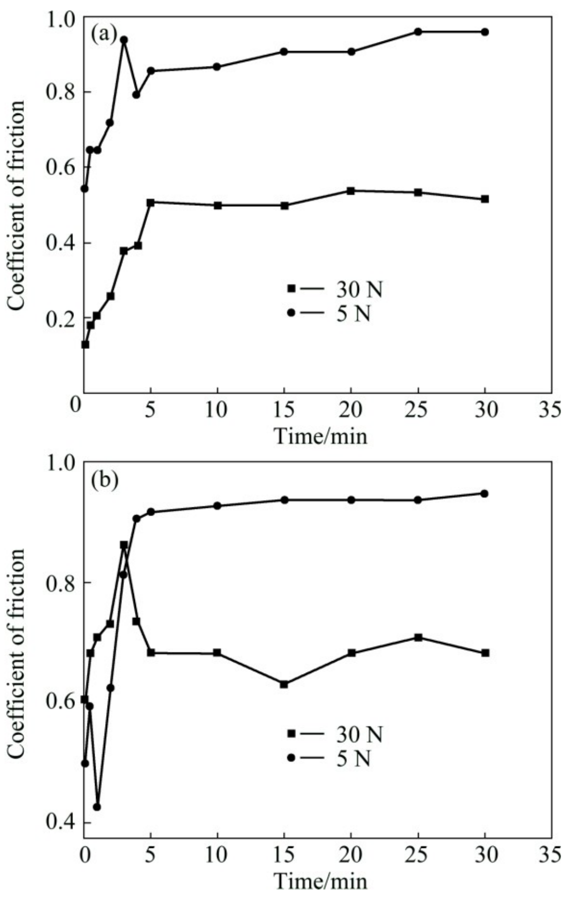

Fig. 7 Evolution of coefficient of friction of coatings as function of sliding time: (a) Couple 1; (b) Couple 2

Figure 8 illustrates the variation of the wear rate as a function of load at a sliding speed of 0.5 m/s for the two couples. In this figure, it can be seen that the wear rate is stable for both couples in the beginning until 20 N. After that, the wear rate increases as the load increases for couple 1. This is due to the allotropic transformation of zirconia from the monoclinic form to the quadratic form which is accompanied by an increasing volume of 5%−9% during the thermal spraying [53]. This causes internal tensions, thus degrades the mechanical properties of couple 1. Therefore, there is the appearance of the third body particles which are rapidly ejected from the friction surface while other particles are oxidized according to the contact temperature. In contrast to couple 2, there is a decreasing of the wear rate after 20 N. It can be explained by the similar chemical compositions of the two surfaces that do not allow the shear mode. We can also conclude that the load affects the tribological properties of the coating with the type of reinforcement.

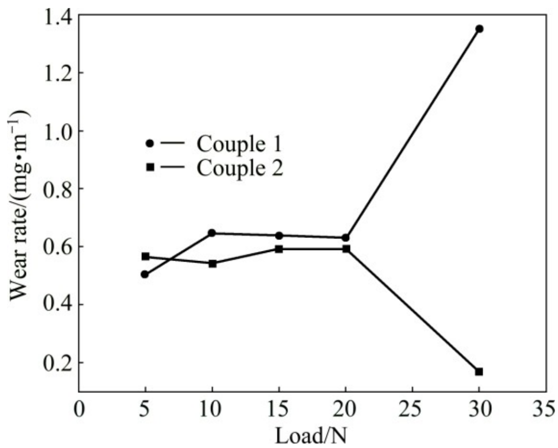

Fig. 8 Evolution of wear rate of coatings as function of load

4 Conclusions

1) The XRD pattern obtained from the wire (AT-3) revealed the presence of three phases: a majority phase of α-Al_2O_3, a secondary phase of $Al_6Si_2O_{13}$ and small amount of rutile α-TiO_2. The XRD pattern of (AT-3) coating also revealed the presence of α-Al_2O_3 phase as matrix and new metastable phase γ-Al_2O_3 and κ-Al_2O_3, but the α-TiO_2 phase had disappeared. By against, the XRD pattern of the composite coating (AZ-25) showed the same phases as the wire: α-Al_2O_3 matrix, monoclinic structure ZrO_2 and a quadratic structure ZrO_2.

2) Characterization of the mechanical properties revealed that AT-3 coating exhibits a higher

microhardness than AZ-25 coating.

3) In most studied conditions, the reinforcement of TiO_2 in AT-3 composite coating displayed a better tribological performance, i.e., lower coefficient of frictions and wear rates, than the reinforcement of ZrO_2 (AZ-25).

References

[1] BERGER L M. Coatings by thermal spray [J]. Comprehensive Hard Materials, 2014, 1: 471−506.

[2] HERMAN H, SAMPATH S, McCUNE R. Thermal spray current status and future trends [J]. MRS Bulletin, 2000, 25(7): 17−25.

[3] PAWLOWSKI L. The science and engineering of thermal spray coatings [M]. 2nd ed. Tokyo: John Wiley and Sons, 1995.

[4] SABIRUDDIN K, BANDYOPADHYAY P P, BOLLELI G, LUSVARGHI L. Variation of splat shape with processing conditions in plasma sprayed alumina coatings [J]. Journal of Materials Processing Technology, 2011, 211(3): 450−462.

[5] KESHRI A K, AGARWAL A. Splat morphology of plasma sprayed aluminum oxide reinforced with carbon nanotubes: A comparison between experiments and simulation [J]. Surface and Coatings Technology, 2011, 206(2−3): 338−347.

[6] ALAMARA K, SAMANDARI S S, STODDART R P, BERNTD C, C. Effect of substrate temperature on the splat formation of flame sprayed polypropylene [J]. Surface and Coatings Technology, 2011, 206(6): 1180−1187.

[7] WANG M, LEON L S. Effects of the powder manufacturing method on microstructure and wear performance of plasma sprayed alumina–titania coatings [J]. Surface and Coatings Technology, 2007, 202(1): 34−44.

[8] KEYVANI A. Microstructural stability oxidation and hot corrosion resistance of nanostructured Al_2O_3/YSZ composite compared to conventional YSZ TBC coatings [J]. Journal of Alloy and Composite, 2015, 623: 229−237.

[9] ZHANG J, KOBAYASHI A. Corrosion resistance of the $Al_2O_3-ZrO_2$ thermal barrier coatings on stainless steel substrates [J].Vacuum, 2008, 83(1): 92−97.

[10] RICO A, RODRIGUEZ J, OTERO E, ZENG P, RAINFORTH W M. Wear behaviour of nanostructured alumina–titania coatings deposited by atmospheric plasma spray [J]. Wear, 2009, 267(5−8): 1191−1197.

[11] LIMARGA M A, SUJANTO W, HON Y T. Mechanical properties and oxidation resistance of plasma-sprayed multilayered Al_2O_3/ZrO_2 thermal barrier coatings [J]. Surface and Coatings Technology, 2005, 197(1): 93−102.

[12] LU X, YAN D R, YANG Y, DONG Y C, HE J N, ZHANG J X. Phase evolution of plasma sprayed Al_2O_3−13%TiO_2 coatings derived from nanocrystalline powders [J]. Transactions of Nonferrous Metals Society of China, 2013, 23(10): 2951−2956.

[13] JIA S K, ZOU Y, XU J Y, WANG J, YU L. Effect of TiO_2 content on properties of Al_2O_3 thermal barrier coatings by plasma spraying [J]. Transactions of Nonferrous Metals Society of China, 2015, 25(1): 175−183.

[14] HE Long, TAN Ye-fa, TAN Hua, ZHOU Chun-hua, GAO Li. Tribological properties of nanostructured Al_2O_3−40%TiO_2 multiphase ceramic particles reinforced Ni-based alloy composite coatings [J]. Transactions of Nonferrous Metals Society of China, 2013, 23(9): 2618−2627.

[15] YOUNES R, BRADAI M A, SADEDDINE A, MOUADJI Y, BILEK A, BENABBAS A. Microstructural and tribological properties of Al_2O_3−13pctTiO_2 thermal spray coatings deposited by flame spraying [J]. Metallurgical and Materials Transactions B, 2015, 46(5): 2394−2403.

[16] GAO Jia-cheng, ZOU Jian, TAN Xiao-wei, WANG Yong. Characteristics and properties of surface coated nano-TiO_2 [J]. Transactions of Nonferrous Metals Society of China, 2006, 16(6): 1252−1258.

[17] ESTILI M, KAWASAKI A, SAKAMOTO H, MEKUCHI Y, KUNO M, TSUKADA T. The homogeneous dispersion of surfactant less, slightly disordered, crystalline, multiwalled carbon nanotubes in α-alumina ceramics for structural reinforcement [J]. Acta Materialia, 2008, 56(15): 4070−4079.

[18] YAO Lei, LIU Jian-hua, YU Mei, LI Song-mei, WU Hao. Formation and capacitance properties of Ti−Al composite oxide film on aluminum [J]. Transactions of Nonferrous Metals Society of China, 2010, 20(5): 825−830.

[19] BAHRAMIAN A, RAEISSI K, HAKIMIZAD A. An investigation of the characteristics of Al_2O_3/TiO_2 PEO nanocomposite coating [J]. Applied Surface Science, 2015, 351(1): 13−26.

[20] PERUMAL G, GEETHA M, ASOKAMANI R, ALAGUMURTHI N. Wear studies on plasma sprayed Al_2O_3−40% 8YSZ composite ceramic coating on Ti−6Al−4V alloy used for biomedical applications [J]. Wear, 2014, 311(1−2): 101−113.

[21] SU Hai-jun, ZHANG Jun, LIU Lin, FU Heng-zhi. Effects of laser processing parameters on solidification microstructures of ternary Al_2O_3/YAG/ZrO_2 eutectic in situ composite and its thermal property [J]. Transactions of Nonferrous Metals Society of China, 2009, 19(6): 1533−1538.

[22] SRINIVASAN P B, LIANG J, BLAWERT C, DIETZEL W. Dry sliding wear behaviour of magnesium oxide and zirconium oxide plasma electrolytic oxidation coated magnesium alloy [J]. Applied Surface Science, 2010, 256(10): 3265−3273.

[23] KHALIL A, KIM S W. Mechanical wet-milling and subsequent consolidation of ultra-fine $Al_2O_3-(ZrO_2+3\%Y_2O_3)$ bioceramics by using high-frequency induction heat sintering [J]. Transactions of Nonferrous Metals Society of China, 2007, 17(1): 21−26.

[24] LIANG B, ZHANG G, LIAO H L, CODDET C, DING C X. Friction and wear behavior of $ZrO_2-Al_2O_3$ composite coatings deposited by air plasma spraying: Correlation with physical and mechanical properties [J]. Surface and Coatings Technology, 2009, 203(20−21): 3235−3242.

[25] OH S T, SEKINO T, NIHARA K. Fabrication and mechanical properties of 5 Vol, percent copper dispersed alumina nanocomposite [J]. Journal of the European Ceramic Society, 1998, 18(1): 31−37.

[26] MISHRA R.S, MUKHEREJEE A K. Processing of high hardness-high toughness alumina matrix nanocomposites [J]. Materials Science and Engineering A, 2001, 301(1): 97−101.

[27] AN J W, YOU D H, LIM D S. Tribological properties of hot-pressed alumina−CNT composites [J]. Wear, 2003, 255(1−6): 677−681.

[28] DATCHEVA M, CHERNEVA S, STOYCHEVA M, IANKOVA R, STOYCHEV D. Determination of anodized aluminum material characteristics by means of nanoindentation measurements [J]. Materials Sciences and Applications, 2011, 2: 1452−1464.

[29] CHERNEVA S, IANKOVA R, RADIC N, GRBIC B, STOYCHEVA D. Nanoindentation investigation of mechanical properties of ZrO_2, $ZrO_2-Y_2O_3$, Al_2O_3 and TiO_2 thin films deposited on stainless steel OC404 substrate by spray pyrolysis [J]. Materials Science and Engineering B, 2014, 183: 12−16.

[30] TAZEGUL O, MUHAFFEL F, MEYDANOGLU O, BAYDOGAN M, KAYALI E S, CIMENOGLU H. Wear and corrosion characteristics of novel alumina coatings produced by micro arc oxidation on AZ91D magnesium alloy [J]. Surface and Coatings Technology, 2014, 258: 168−173.

[31] KIM S H, HANNULA S P, LEE S W. Effects of the sliding conditions on the tribological behavior of atmospheric plasma sprayed Al_2O_3−15wt% ZrO_2-CaF_2 composite coating [J]. Surface and Coatings Technology, 2012, 210: 127−134.

[32] ZHOU Yue-bo, CHEN Hong-yu, ZHANG Hai-jun, WANG Yong-dong. Oxidation of Al_2O_3-dispersion chromizing coating by pack-cementation at 800 °C [J]. Transactions of Nonferrous Metals Society of China, 2008, 18(3): 598−602.

[33] ZHAO Xiao-qin, AN Yu-long, CHEN Jian-min, ZHOU Hui-di, YIN Bin. Properties of Al_2O_3−40wt%ZrO_2 composite coatings from ultra-fine feedstocks by atmospheric plasma spraying [J]. Wear, 2008,

265(11−12): 1642−1648.

[34] VOLCEANOV E, VOLCEANOV A, STOLERIU Ş. Assessment on mechanical properties controlling of alumina ceramics for harsh service conditions [J]. Journal of European Ceramic Society, 2007, 27: 759−762.

[35] HORI S, KURITA R, YOSHIMURA M, SOMIYA S. Suppressed grain growth in final stage sintering of Al_2O_3 with dispersed ZrO_2 particles [J]. Journal of Materials Science Letters, 1985, 4(9): 1067−1070.

[36] MESSING L G, KUMANGI M. Low-temperature sintering of seeded sol-gel derived, ZrO_2-toughened Al_2O_3 composites [J]. Journal of the American Ceramic Society, 1989, 72(1): 40−44.

[37] SRDIC V V, RADONJIC L. Transformation toughening in sol-gel-derived alumina-zirconia composites [J] Journal American of Ceramic Society, 1997, 80(8): 2056−2060.

[38] WANG J, STEVENS R. Review zirconia-toughened alumina (ZTA) ceramics [J]. Journal of Materials Science, 1989, 24: 3421−3440.

[39] FERVEL V, NORMAN B, CODDET C. Tribological behavior of plasma sprayed Al_2O_3-based cermet coatings [J]. Wear, 1999, 230(1): 70−77.

[40] HABBIB K A, SAURA J J, FERRE C, DAMRA M S, GIMENEZ E, CABEDO L. Comparison of flame sprayed Al_2O_3/TiO_2 coatings: Their microstructure, mechanical properties and tribology behavior [J]. Surface and Coating Technolgy, 2006, 201(3−4): 1436−1443.

[41] AHN J, WANG B H, SONG E P, LEE S, KIM N J. Correlation of microstructure and wear resistamce of Al_2O_3–TiO_2 coating plasma sprayed with nanopowders [J]. Metall Mater Trans A, 2006, 37(6): 1851−1861.

[42] Standard ASTM C1327-99. Standard test method for Vickers indentation hardness of advanced ceramics [S].

[43] HOCHAUEUR D, MITTERER C, PENOY M, MICHOTTE C, MARTINEZ H P, KATHREIN M. Thermal stability of doped CVD κ-Al_2O_3 coatings [J]. Surface and Coatings Technology, 2010, 204(21−22): 3713−3722.

[44] ÖHMAN L O, PAUL J. Materials aspects of titanium-doped aluminas: 14%Ti/γ-Al_2O_3/Cu and sulfided Al_2O_3–TiO_2/NiMo [J]. Materials Chemistry and Physics, 2002, 73(2−3): 242−251.

[45] GAO Jun-guo, HE Ye-dong, GAO Wei. Oxidation behavior of γ-TiAl based alloy with Al_2O_3−Y_2O_3 composite coatings prepared by electrophoretic deposition [J]. Surface and Coatings Technology, 2011, 205(19): 4453−4458.

[46] TURAN W H, CHEN R Z, WANG T C, CHENG C H, KUO P S. Mechanical properties of Al_2O_3/ZrO_2 composites [J]. Journal European of Ceramic Society, 2002, 22(16): 2827−2833.

[47] HANNINK R H J, KELLY P M, MUDDLE B C. Transformation toughening in zirconia containing ceramics [J]. Journal of American Ceramic Society, 2000, 83: 461−487.

[48] IANKOV R, CHERNEVA S, STOYCHEV D. Investigation of material properties of thin copper films through finite element modeling of microindentation test [J]. Applied Surface Science, 2008, 254(17): 5460−5469.

[49] FERVEL V, NORMAND B, CODDET C. Tribological behavior of plasma sprayed Al_2O_3-based cermet coatings [J]. Wear, 1999, 230(1): 70−77.

[50] HABIB K A, SAURA J J, FERRE C, DAMRA M S, GIMENEZ E, CABEDO L. Comparison of flame sprayed Al_2O_3/TiO_2 coatings: Their microstructure, mechanical properties and tribology behavior [J]. Surface and Coatings Technology, 2006, 201(3−4): 1436−1443.

[51] PALACIO C C, AGEORGES H, VARGAS F, DIAZ A F. Effect of the mechanical properties on drilling resistance of Al_2O_3–TiO_2 coatings manufactured by atmospheric plasma spraying [J]. Surface and Coatings Technology, 2013, 220(15): 144−148.

[52] YILMAZ R, KURT A O, DEMIR A, TATLI Z. Effects of TiO_2 on the mechanical properties of the Al_2O_3–TiO_2 plasma sprayed coating [J]. Journal of the European Ceramic Society, 2007, 27(2−3): 1319−1323.

[53] JORAND Y. Preparation and characterization of composite dispersoids ternary alumina−zirconia based thermomechanical purpose [D]. National Institute of Applied Sciences, Lyon University, France, 1991: 334.

添加 TiO_2 和 ZrO_2 对火焰热喷涂 Al_2O_3 涂层性能的影响

Rassim YOUNES[1], Mohand Amokrane BRADAI[1], Abdelhamid SADEDDINE[1],
Youcef MOUADJI[2], Ali BILEK[3], Abderrahim BENABBAS[4]

1. Laboratory of Mechanics, Materials and Energetic, Faculty of Technology, University of Bejaia, 06000 Bejaia, Algeria;
2. Laboratory of Mechanics, Faculty of Engineering Sciences, Campus Chaabet-Ersas, University of Constantine, 25000 Constantine, Algeria;
3. Mechanical Laboratory of Structure and Energetic, Mechanical Engineering Department, University of Tizi-Ouzou, 15000 Tizi-Ouzou, Algeria;
4. Laboratory Processes for Materials, Energy, Water and Environment, Faculty of Science and Technology, University of Bouira, 10000 Bouira, Algeria

摘　要：采用火焰热喷涂技术在低碳钢表面上沉积制备添加 25% ZrO_2(简称 AZ-25)和 3% TiO_2(简称 AT-3)增强体的 Al_2O_3 涂层，对涂层的显微组织、相组成、显微硬度和摩擦学性能进行了研究。X 射线衍射(XRD)结果表明，AT-3 涂层的主要相组成为 α-Al_2O_3，此外还含有一些亚稳的 β-Al_2O_3 和 κ-Al_2O_3 相。而 AZ-25 涂层的主要相组成为 α-Al_2O_3，还有一些 q-ZrO_2 和 m-ZrO_2 相。在大多数实验条件下，AT-3 涂层的摩擦学性能(摩擦因数、磨损率)均比 AZ-25 涂层要好。添加 ZrO_2 增强体会导致涂层的显微硬度降低，而添加 TiO_2 会使涂层硬度增加。

关键词：热喷涂；涂层；增强体；摩擦因数；磨损率

(Edited by Sai-qian YUAN)